Macroscopic permeability of three-dimensional fracture networks with power-law size distribution

V. V. Mourzenko, J. -F. Thovert, P. M. Adler

HAL Id: insu-03600283
https://insu.hal.science/insu-03600283

Submitted on 8 Mar 2022

Macroscopic permeability of three-dimensional fracture networks with power-law size distribution

V. V. Mourzenko,[1] J.-F. Thovert,[1] and P. M. Adler[2]

[1]*LCD-CNRS, SP2MI, Boîte Postale 179, 86960 Futuroscope Cedex, France*
[2]*IPGP, tour 24, 4 Place Jussieu, 75252 Paris Cedex 05, France*

Fracture network permeability is investigated numerically by using a three-dimensional model of plane polygons uniformly distributed in space with sizes following a power-law distribution. Each network is triangulated via an advancing front technique, and the flow equations are solved in order to obtain detailed pressure and velocity fields. The macroscopic permeability is determined on a scale which significantly exceeds the size of the largest fractures. The influence of the parameters of the fracture size distribution—the power-law exponent and the minimal fracture radius—on the macroscopic permeability is analyzed. Eventually, a general expression is proposed, which is the product of a dimensional measure of the network density, weighted by the individual fracture conductivities, and of a fairly universal function of a dimensionless network density, which accounts for the influences of the fracture shapes and of the parameters of their size distribution. Two analytical formulas are proposed which successfully fit the numerical data over a wide range of network densities.

I. INTRODUCTION

Fractures and fracture networks determine the permeability of many natural rocks, and their behavior has drawn attention in various fields; different aspects of this problem are discussed by, e.g., Sahimi [1], Adler and Thovert [2], and the National Research Council [3].

In our previous contributions, the geometrical properties [4], the absolute permeability of fracture networks [5] and of fractured porous media [6], as well as their relative permeabilities [7] have been determined for monodisperse fractures. It has been shown that the excluded volume introduced by Balberg *et al.* [8] plays a crucial role; a dimensionless fracture density ρ' was defined and the previous properties depend only on ρ' whatever the shape of the fractures.

However, it has been known for a long time that real fracture networks are polydisperse [9–13]. Therefore, the main objective of this paper is to extend the results of Koudina *et al.* [5] to three-dimensional fracture networks with a power-law size distribution.

To the best of our knowledge (see the recent review of Berkowitz [14]), there is no such previous study on three-dimensional permeability.

Renshaw [15] discussed the applicability of different effective medium models to the prediction of the macroscopic permeability of fractured networks. He demonstrated that these models fail for the range of fracture spatial densities observed on superficial exposures of joint networks. He studied numerically the permeability of two-dimensional power-law networks of orthogonal fractures and used a fracture density parameter based on the second moment of the length distribution; he proposed a normalized permeability in order to gather all the numerical results.

A numerical study of the flow in two-dimensional fracture networks has been performed by Odling [16]. Special attention was paid to the influence of the correlation between fracture lengths and conductivities on the macroscopic permeability; she found that correlated fracture apertures and lengths induce global permeabilities an order of magnitude greater than when aperture and lengths are uncorrelated or when apertures are identical.

De Dreuzy *et al.* [17] (and the references therein) also considered two-dimensional networks with various properties of the individual fractures.

In the present study, the fracture network permeability is considered numerically by using a three-dimensional model of plane polygons uniformly distributed in space with sizes following a power-law distribution. The domain size is supposed to significantly exceed the size of the largest fractures in the networks. The presentation is organized as follows. In Sec. II, the geometrical model of polydisperse fracture networks is described together with the flow equations; the numerical approach is briefly discussed. Each network is triangulated via an advancing front technique; the flow equations are discretized on this mesh and solved in order to obtain the pressure and velocity fields. The macroscopic flow is related by an effective permeability to the pressure gradient imposed on the system; this permeability is averaged over a number of independent statistical realizations of fracture networks with the same properties. Percolation properties of polydisperse fracture networks are presented in Sec. III. In Sec. IV, the influence of the parameters of the fracture size distribution—the power-law exponent a and the minimal fracture radius—on the macroscopic permeability is analyzed for fractures with identical conductivities. The results are systematically presented in terms of the ratio of the network permeability to the fracture surface density and of the third moment of the fracture size distribution. For variable fracture conductivities, which are addressed in Sec. V, two models are considered—polydisperse networks with fracture conductivities scaling with the fracture size, and monodisperse systems with conductivities distributed according to a power law. Some concluding remarks in Sec. VI complete this paper.

The main findings can be summarized by the general expression Eq. (37) for the macroscopic permeability, together with the models Eqs. (38) and (42) for the universal function of the dimensionless network density defined in Eq. (6c).

II. GENERAL

Consider three-dimensional networks made of fractures that are disks or regular polygons circumscribed by disks of radius R. According to various observations of fractured rocks ([2] and the references herein), many real probability densities of fracture sizes follow a power law such as

$$n(R) = \alpha R^{-a} \qquad (1)$$

where $n(R)dR$ is the number of fractures with radius in the range $[R, R+dR]$, α is a coefficient, and a a scaling exponent. In practice, R varies in a large interval of values which can span five orders of magnitude, but it is limited by the size R_M of the largest fractures in the system and by the size R_m of the microcracks. Moreover, the normalization condition implies that α satisfies

$$\alpha = \frac{a-1}{R_m^{1-a} - R_M^{1-a}}. \qquad (2)$$

According to a recent synthesis of the real distribution of fracture trace lengths in a plane intersecting a three-dimensional fracture network, the corresponding exponent a_{2D} varies between 0.8 and 3.5 with a maximum occurrence around 2.0 [18]. Piggott [19] argued via an analytical development that the exponents a_{2D} and a are related by $a = a_{2D} + 1$; a similar observation in numerical simulations has been presented by Berkowitz and Adler [20]. Thus, it is reasonable to expect that a varies between 1.8 and 4.5 with a maximum likelihood around 3.0.

The volumetric density $F(R)$ is defined as the number of fractures of size R in a unit volume

$$F(R) = \rho n(R) \qquad (3)$$

where the total fracture number per unit volume is ρ. A more intrinsic measure of the density can be devised by combining ρ with the excluded volume V_{ex} introduced by Balberg et al. [8]; V_{ex} is defined as the surrounding volume into which the center of another object may not enter if overlap is to be avoided. For anisotropic objects such as polygons, V_{ex} depends on their mutual orientation, and it has to be averaged over all possible orientations. For a wide class of objects including randomly oriented disks or convex polygons, an exact expression for V_{ex} was given by Huseby et al. [4]:

$$V_{ex} = A_p P_p / 2 \qquad (4)$$

where A_p and P_p are the polygon area and perimeter. For disks with radius R, Eq. (4) gives $V_{ex} = \pi^2 R^3$ [21].

For monodisperse fracture networks, the dimensionless density $\rho' = \rho V_{ex}$, which is the number of fractures per excluded volume V_{ex}, has been shown to characterize well the network connectivity of fractures of various shapes; a unique percolation threshold was obtained as $\rho'_c = 2.26 \pm 0.04$ [4].

It should be noted that ρ' is a direct measure of the network connectivity, since it is exactly equal to the mean number of intersections of a fracture with others in the network. For the networks under consideration here, which are made

up of fractures with identical shapes but different sizes, it is convenient to express the excluded volume V_{ex} in Eq. (4) as the product

$$V_{ex} = v_{ex} R^3, \qquad (5)$$

where v_{ex} is a dimensionless shape factor, equal, for instance, to π^2 for disks, $9\sqrt{3}/2$ for hexagons, and $4\sqrt{2}$ for squares. It was the introduction of this shape factor in the density ρ' that allowed unification of the description of the percolation and transport properties of monodisperse networks of fractures with various shapes. Therefore, this feature is kept in the definitions of the three dimensionless densities that are used in the following:

$$\rho'_0 = \rho v_{ex} R_M^3, \qquad (6a)$$

$$\rho'_{21} = \rho v_{ex} \langle R^2 \rangle \langle R \rangle, \qquad (6b)$$

$$\rho'_3 = \rho v_{ex} \langle R^3 \rangle, \qquad (6c)$$

where the brackets $\langle \rangle$ denote statistical moments of R weighted by $n(R)$. The subscripts are reminders of the statistical moments involved in each definition. The first one, ρ_0', is the simplest definition, based on the single length scale R_M, but it cannot be expected to capture the scaling character of the network. The second one is the generalization of ρ' for monodisperse networks, since it can be shown that it is still equal to the mean number of intersections per fracture [2]. It is therefore a suitable candidate, but it turns out that this measure of the local connectivity does not control the global network percolation and that the last one ρ'_3 is much more successful in this respect, as was established earlier [21–23].

The generation and analysis of the percolation properties of fracture networks are similar to those presented by Huseby et al. [4]. The fractures are embedded in the unit cubic cell of size L; $N_{fr} = \rho L^3$ is the number of fractures in the unit cell. The centers of the fractures are uniformly distributed in space, and their normal vectors are uniformly distributed on the unit sphere.

In this study, only large unit cells $L \geq 4R_M$ are considered. This means that L is a natural homogenization scale over which the macroscopic permeability of a fracture network can be defined. Any scaling behavior of hydraulic properties of fracture systems which can arise when L varies in the range $L \ll 4R_M$ is beyond the scope of the current analysis.

Two types of fracture systems were used in the calculations depending on the boundary conditions. First, nonperiodic networks were tested, so that percolation requires that a connected cluster joins opposite faces of the unit cell along, say, the x direction; in this case, fracture centers were generated within the unit cell as well as outside it, provided that the corresponding fractures intersect at least one of the six faces of the cell. Second, spatially periodic networks were generated; all fracture centers lie in the interior of the unit cell τ_0; then, percolation is ensured if a connected cluster contains two homologous fractures, i.e., two fractures with the same coordinates, modulo the period L along the corresponding direction.

The three length scales define the two dimensionless ratios

$$\frac{R_m}{R_M}, \quad \frac{L}{R_M},\tag{7}$$

which together with a determine the connectivity and percolation properties of the fracture networks. In order to eliminate the influence of the lower cutoff R_m, R_m/R_M is kept as small as possible.

At a local scale characterized by a typical aperture b, the flow of a Newtonian fluid within a fracture is governed by the Stokes equation. If b is assumed to be much smaller than the typical lateral extent $2R$ of the fracture, flow at a scale that is intermediate between b and $2R$ is governed by the Darcy equation

$$\mathbf{q} = -\frac{1}{\mu}\sigma\overline{\mathbf{\nabla}p}\tag{8}$$

where $\mathbf{q}$ is the locally averaged flow rate per unit width $[L^2T^{-1}]$, μ the fluid viscosity, $\overline{\mathbf{\nabla}p}$ the pressure gradient, and $\sigma\,[L^3]$ the fracture conductivity coefficient. The mass conservation equation becomes

$$\mathbf{\nabla}_s \cdot \mathbf{q} = 0\tag{9}$$

where $\mathbf{\nabla}_s$ is the two-dimensional gradient operator in the mean fracture plane.

Two types of boundary conditions can be applied to this network. For periodic systems of fractures, a macroscopic pressure gradient $\overline{\overline{\mathbf{\nabla}p}}$ is applied upon the unbounded medium made of the periodic juxtaposition of identical unit cells τ_0 along the three directions of space. The fluid flow is described by Eqs. (8) and (9), together with periodic conditions for the local velocity $\mathbf{v}$, $\mathbf{q}$, and $\mathbf{\nabla}p$; $\overline{\overline{\mathbf{\nabla}p}}$ can be expressed as

$$\overline{\overline{\mathbf{\nabla}p}} = \frac{1}{\tau_0}\int_{\partial\tau_0}p\,d\mathbf{s}.\tag{10}$$

The seepage velocity $\bar{\mathbf{v}}$ can be evaluated as

$$\bar{\mathbf{v}} = \frac{1}{\tau_0}\int_{\tau_f}\mathbf{v}\,d\tau = \frac{1}{\tau_0}\int_{S_f}\mathbf{q}\,d\mathbf{S},\tag{11}$$

where τ_f is the interstitial volume of the fractures and S_f their projection on their mean planes. The flux is related to the pressure gradient by Darcy's law [2]

$$\bar{\mathbf{v}} = -\frac{1}{\mu}\mathbf{K}\cdot\overline{\overline{\mathbf{\nabla}}}p.\tag{12}$$

$\mathbf{K}$ is the permeability tensor $[L^2]$, to be determined from Eqs. (11) and (12) once the problem of Eqs. (8) and (9) has been solved. Since all the networks considered here are isotropic, $\mathbf{K}$ is a spherical tensor when averaged over many realizations,

$$\mathbf{K} = K\mathbf{I}.\tag{13}$$

Such periodic conditions have been applied in a few cases, but, unless otherwise stated, most calculations in the following have been conducted for nonperiodic systems of fractures; prescribed pressures were then applied over some inlet and outlet planes $\mathcal{P}_i$ and $\mathcal{P}_o$,

$$p = -\left(\overline{\overline{\mathbf{\nabla}}}p\right)_\alpha L \text{ along } \mathcal{P}_{i\alpha},$$

$$p = 0 \text{ along } \mathcal{P}_{o\alpha}, \quad \alpha = x,y,z.\tag{14}$$

A no-flux condition is applied over the other panes bounding the unit cell. The flow calculations are successively performed along the three different directions, and the macroscopic permeability of the network is derived from Eqs. (11) and (12). In this case, $\mathbf{K}$ is not a tensor, but for isotropic networks its statistical average is still expected to be spherical.

In this paper, σ is taken to be constant over each fracture. Because of the classical Poiseuille law, the typical conductivity σ_0 of a fracture is expected to be of the order of

$$\sigma_0 = \frac{b^3}{12}.\tag{15}$$

This value, together with R_M and a reference pressure p_0, are used to recast the equations in a dimensionless form. The dimensionless parameters (with primes) are defined by

$$p = p_0 p', \quad \mathbf{\nabla} = \frac{1}{R_M}\mathbf{\nabla}', \quad \mathbf{v} = \frac{\sigma_0 p_0}{\mu R_M^2}\mathbf{v}',$$

$$\mathbf{q} = \frac{\sigma_0 p_0}{\mu R_M}\mathbf{q}', \quad \sigma = \sigma_0\sigma\prime, \quad \mathbf{K} = \frac{\sigma_0}{R_M}\mathbf{K}',\tag{16}$$

$$R_m = R_M R_M', \quad L = R_M L', \quad R = R_M R'.$$

Other choices are of course possible for the units, but since Eqs. (8) and (9) are linear, the results would not be essentially different. For instance, the velocity unit could be $\sigma_0 p_0/\mu R_M b$, which yields a dimensionless interstitial velocity of order 1, whereas the definition in Eq. (16) yields a seepage velocity $\bar{v}\prime$ of order 1.

All the following developments use this dimensionless formulation; our results will be presented in terms of the dimensionless scalar permeability K'.

A numerical method applied to solve the flow problem was described by Koudina *et al.* [5]. First, the fracture network is discretized; an unstructured triangulation of the fractures is obtained by using an advancing front technique. Since the triangular mesh is made to coincide with the fracture intersection lines, which are randomly located, it generally contains triangles of various sizes and shapes. The mesh is characterized by the prescribed maximum edge length δ_M, which is set equal to $R_M/4$ in most cases. Hence, an hexagonal fracture with $R=R_M$ contains at least 61 nodes and 96 equilateral triangles, in the unlikely case when it intercepts no other fracture, and more typically about 100 nodes and 140 scalene triangles when the mesh is constrained by intersection lines. Small fractures with R of the order of δ_M or

smaller contain at least four triangles. Let us give an example of the mesh sizes used in this study; a network with $a=2.5$, $R'_m=0.1$, $L'=4$, and $\rho'_3=12$ contains approximately 4000 fractures with 100 000 triangles and 50 000 nodes.

The pressure p is determined at each point of the triangular mesh. The unknown pressures are determined by solving the linear algebraic equations derived by the finite volume technique.

For each set of model parameters, the flow simulations have been performed on $N_r=25$ realizations of fracture networks. Unless otherwise stated, the macroscopic permeabilities given in the following are always averages over these N_r realizations and over the three directions x, y, and z. Nonpercolating networks with zero macroscopic permeability are also taken into account in the statistical averaging.

III. PERCOLATION PROPERTIES OF FRACTURE NETWORKS

These properties were derived by using the same approach as Huseby et al. [4]. For given values of ρ'_0, L', and a, the probability $\Pi(L',a,\rho'_0)$ of having a percolating cluster which spans the cell in the x direction is derived from N_r realizations of the system; then, the value $\rho'_{0c}(L')$ for which $\Pi=0.5$ is estimated. In all tests, the value $N_r=500$ is used.

In the limit of small R_M/L and at fixed R_m, the fracture networks are expected to follow the standard percolation theory with the percolation threshold $\rho'_{0c}(\infty)$ [24]:

$$\rho'_{0c}(L') - \rho'_{0c}(\infty) \propto \left(\frac{1}{L'}\right)^{1/\nu}, \tag{17}$$

where ν is the critical exponent. In our estimations of $\rho'_{0c}(L')$, the data for $\Pi(L',a,\rho'_0)$ were fitted with a two-parameter error function of the form

$$\Pi(L',a,\rho'_0) = \frac{1}{\sqrt{2\pi}} \int_{-\infty}^{\rho'_0} \frac{1}{\Delta_L} \exp\left[\frac{-[\xi-\rho'_{0c}(L')]^2}{2(\Delta_L)^2}\right] d\xi, \tag{18}$$

where Δ_L is the width of the transition region of $\Pi(L',a,\rho'_0)$.

In practice, the percolation probability $\Pi(L',a,\rho'_0)$ was evaluated from sets of 500 realizations, for about 10 values of the network density, evenly distributed in a range where Π varies from 0.05 to 0.95. Since there is a correspondence between ρ'_0, ρ'_{21}, and ρ'_3, for given values of a and R_m, the same data sets can be used to determine $\rho'_{0c}(L)$, $\rho'_{21c}(L)$, and $\rho'_{3c}(L)$. The 95% confidence interval is estimated to be about ± 0.04 in terms of $\rho'_{3c}(L)$.

The scaling law Eq. (17) can also be used to determine the exponent ν from the values of $\rho'_{0c}(L')$ for various sample sizes. However, percolation is not the main topic of this paper, and such a finite size effect analysis was not conducted.

In order to compare the results for fracture networks with various R'_m, we have to choose the parameters that will be kept constant. ρ'_3 was suggested to be the appropriate percolation parameter in previous studies [21–23], which also stressed the importance of the large scale part of the fracture distribution for the network connectivity. The numerical

simulations performed in this study on the three-dimensional percolation in power law fracture systems showed that this is indeed true in the range $L'>1$, as confirmed by the following analysis of the dependence of various percolation parameters on the lower cutoff length.

Figure 1 shows the percolation threshold as a function of R'_m. Three different definitions of the critical fracture network density are considered, namely, the thresholds $\rho'_{0c}(L')$, $\rho'_{21c}(L')$, and $\rho'_{3c}(L')$ associated with the three dimensionless densities in Eq. (6), and they give rise to very different trends which can be rationalized as follows.

When R_M and ρ'_0 are kept constant and R_m decreases, the same number of fractures is spread over a wider range of sizes, and large fractures are replaced by smaller ones. For instance, if follows from Eqs. (1)–(3) that the density of the largest fractures decreases as

$$F(R_M) \sim R_m^{a-1}. \tag{19}$$

This is obviously unfavorable for percolation and therefore ρ'_{0c} has to increase when R_m decreases, as observed in Fig. 1(a).

If instead ρ'_{21}, i.e., the mean number of intersections per fracture, is kept constant and R_m decreases, it implies that the number of large fractures (with many intersections) increases, in order to compensate for the larger number of small fractures with less than the average intersections. Specifically,

$$F(R_M) \propto R_m^{1-a}, \quad 1 < a < 2, \tag{20a}$$

$$F(R_M) \propto R_m^{-1}, \quad 2 < a < 3, \tag{20b}$$

$$F(R_M) \propto R_m^{a-4} \quad 3 < a < 4. \tag{20c}$$

This favors percolation, and therefore ρ'_{21c} decreases when R_m decreases, as seen in Fig. 1(b).

Finally, both $\langle R^3 \rangle$ and the density of large fractures scale as R_m^{a-1} for $1 < a < 4$. This means that the density of large fractures is nearly unaffected when R_m decreases and ρ'_3 is kept constant. In other words, the density ρ'_3 is almost insensitive to the value of the lower cutoff R_m, provided that it is much smaller than R_M. Since the threshold $\rho'_{3c}(L')$ is also nearly independent of R_m in Fig. 1(c), it suggests that for $a<4$ percolation relies on the upper part of the fracture size spectrum.

Let us consider now in more detail $\rho'_{3c}(L')$, which has the crucial advantage of being almost independent of a and R'_m [Fig. 1(c)]. For monodisperse networks, $R'_m=1$, the percolation threshold does not depend on a, but it varies with the scale, when L' increases from 4 to 6. The finite size effect, which is still relatively strong for $L'=4$, can explain the small differences observed in the numerical values of $\rho'_{3c}(L')$ for periodic and nonperiodic networks as well as between hexagons and squares. When R'_m starts decreasing from unity, $\rho'_{3c}(L')$ also decreases a little, but when R'_m becomes less than about 0.1, $\rho'_{3c}(L')$ remains nearly constant and only slightly smaller than the value for monodisperse networks. The only exception is the case $a=2.9$ for which the critical
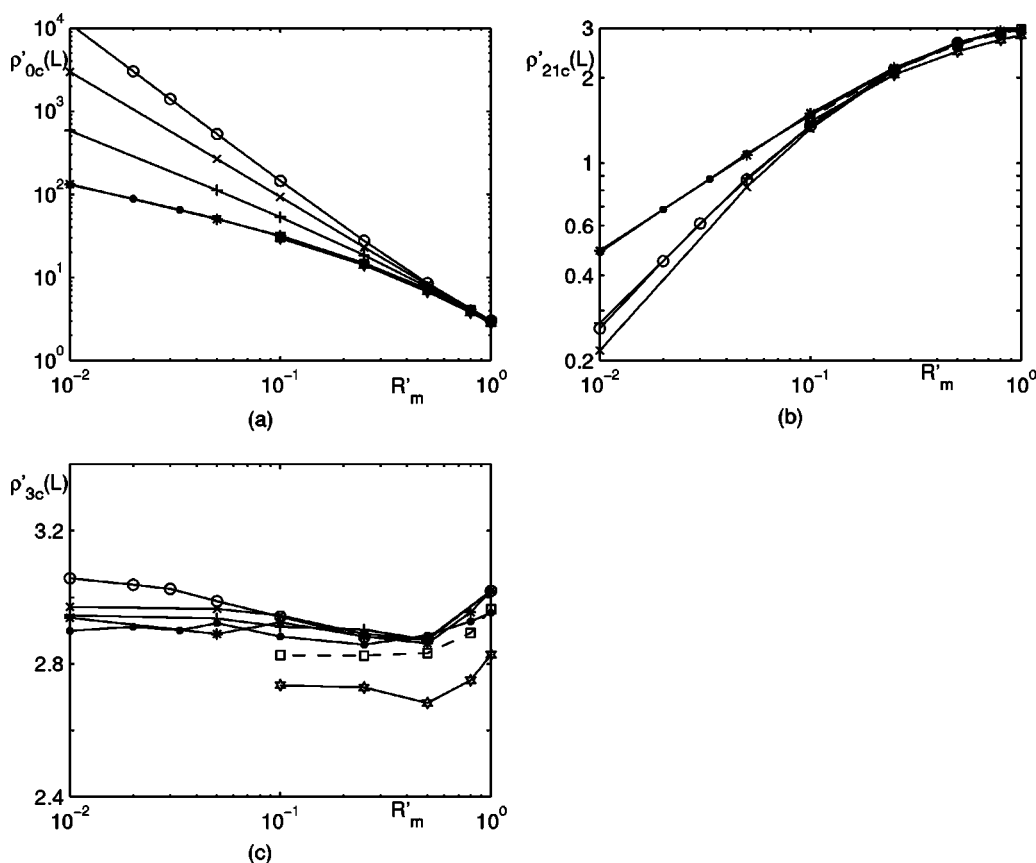
FIG. 1. Percolation thresholds expressed in terms of the densities $\rho'_{0c}(L')$ (a), $\rho'_{21c}(L')$ (b), and $\rho'_{3c}(L')$ (c) for regular hexagons versus R'_m in nonperiodic networks with $L'=4$ and $a=1.5$ (∗), $a=2$ (+), $a=2.5$ (×), $a=2.9$ (○) and with $L'=6$ and $a=1.5$ (☆); data for square fracture are also shown for $L'=4$, $a=1.5$ (□). Data for periodic networks with $L'=4$ and $a=1.5$ (●) are presented for regular hexagons.

density ρ'_{3c} has not yet reached an asymptotic value when R'_m has decreased to 0.03. This is probably because the influence of the smallest fractures is slower to vanish, since their proportion is very large for $a=2.9$.

In summary, for all the data in Fig. 1(c) for $L'=4$, which include different fracture shapes, exponents a from 1.5 to 2.9, and size ranges with R_m/R_M from 0.01 to 1,

$$\rho'_{3c} = 2.95 \pm 0.1 \ (L'=4). \tag{21}$$

Although this value is still relatively strongly influenced by the finite sample size—recall that a critical density 2.30 is expected for monodisperse hexagons when $L' \rightarrow \infty$ [4]—this very narrow range illustrates how successfully the definition (6c) of ρ'_3 incorporates the effect of the fracture shape (via v_{ex}) and of the parameters a and R'_m (via the moment $\langle R'^3 \rangle$).

IV. PERMEABILITY OF FRACTURE NETWORKS WITH IDENTICAL CONDUCTIVITIES

A. Snow model

Let us recall first the theoretical results relative to networks of infinite plane channels with an arbitrary orientation distribution [25,26]. This is equivalent to assuming that all the fracture surfaces in the network contribute to the flow and that the overall head gradient is uniformly distributed over the entire flow domain. If the surface area per unit volume for the fractures normal to **n** is $S(\mathbf{n})$, the permeability tensor is given by

$$\mathbf{K}_{Sn} = \sigma \int S(\mathbf{n})(\mathbf{I} - \mathbf{nn})d\mathbf{n}. \tag{22}$$

For an isotropic network, $S(\mathbf{n})=S/4\pi$ where S is the total volumetric surface area and **n** is evenly distributed on the unit sphere. Therefore,

$$\mathbf{K}_{Sn} = K_{Sn}\mathbf{I}, \ K_{Sn} = \tfrac{2}{3}\sigma S. \tag{23}$$

In random network with fractures of the same size and shape, S is given by

$$S = \rho A_p, \tag{24}$$

and the dimensional permeability can be written in the form

$$K_{Sn} = \tfrac{2}{3}\rho \sigma A_p. \tag{25}$$

If the fracture sizes follow Eq. (1), the total volumetric area S is given by

$$S = \int_{R_m}^{R_M} A_p(R)F(R)dR = \rho \int_{R_m}^{R_M} A_p(R)n(R)dR = \rho\langle A_p\rangle.$$

$$(26)$$

where the brackets $\langle\ \rangle$ denote an average over the size R. Equation (23) then yields a generalized form of Eq. (25),

$$K_{Sn} = \tfrac{2}{3}\rho\sigma\langle A_p\rangle. \tag{27}$$

Note finally for later use that if σ is not identical for all the fractures, Eq. (22) can be generalized by assuming that the contributions of fractures with different conductivities to the total flow are independent, and by averaging it over σ. If σ is correlated with the fracture size R, as in Eq. (33), this yields

$$K_{Sn} = \tfrac{2}{3}\rho\langle\sigma A_p\rangle, \quad \langle\sigma A_p\rangle = \int_{R_m}^{R_M} \sigma(R)A_p(R)n(R)dR, \quad (28)$$

which generalizes both Eq. (25) and Eq. (27).

The macroscopic permeability of Eqs. (23), (25), (27), and (28) relies on the assumptions that there is no flow interaction between the various fractures and that the flow domain includes the whole surface area of the fracture system. For monodisperse fractures, this is true for networks with a large density [5]. In many other cases, these assumptions are not verified and the variations of K with the surface area are not linear. However, it seems reasonable to use the weighted fracture surface area $\rho\langle\sigma A_p\rangle$ as a natural measure of the macroscopic permeability of a fracture network.

B. Numerical results

As stated above, fracture networks with a constant fracture conductivity $\sigma'=1$ are analyzed. For the sake of uniformity of the presentation, the notation of fracture conductivity σ is kept in the factor $\rho\langle\sigma A_p\rangle$ throughout this section.

Examples of results for monodisperse networks and polydisperse networks with $a=1.5$ and $a=2.9$ are presented in Fig. 2. It shows that very different values of K' are obtained for the same ρ_3', which is at least partly due to substantial differences in the total fracture surface. In order to reduce this influence, and as suggested by Eq. (28), the results of this study will be presented henceforth in terms of the normalized permeability

$$K_2' = \frac{K}{\rho\langle\sigma A_p\rangle}. \tag{29}$$

The subscript 2 corresponds to the statistical moment of R used in the normalization [see Eq. (6)]. Note that in these terms Snow's model Eq. (28) is reduced to

$$K_2'(Sn) = \tfrac{2}{3}, \tag{30}$$

and it does not depend either on the fracture size distribution or on the fracture conductivities. A similiar approach has been used by Hestir and Long [27], who developed percolation and effective medium models for two-dimensional fracture networks and proposed analytical expressions which relate the ratio Eq. (29) to a connectivity parameter, namely,
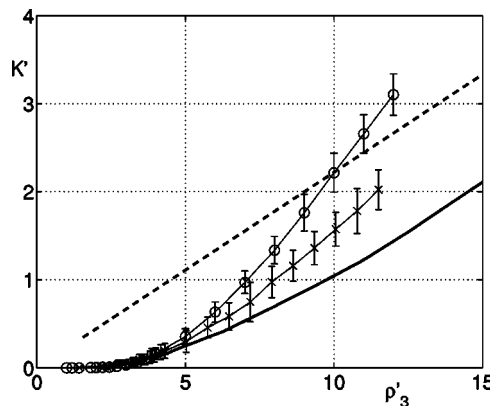

FIG. 2. Permeability K' for nonperiodic networks of regular hexagons versus ρ_3' for $R_m'=0.1$, $L'=4$, $a=1.5$ ($\times$) and $a=2.9$ ($\bigcirc$). Each point is the average over 25 realizations; the vertical bars correspond to the standard deviation of the numerical results. The thick solid line corresponds to monodisperse fracture networks and the thick broken line to the Snow equation Eq. (28) for monodisperse fracture networks.

the average number of intersections per fracture.

Let us consider first the results plotted in Fig. 3(a) for monodisperse networks of regular hexagons, for which $\langle\sigma A_p\rangle$ is reduced to $3\sqrt{3}(\sigma_0 R_M^2)/2$. Monodisperse fracture networks were analyzed by Koudina *et al.* [5]; the additional numerical data presented here for such networks include higher densities which can now be explored due to progress of the numerical technique and of computing capabilities. The nonlinear behavior of the macroscopic permeability K' with the fracture density is well observed; K' asymptotically approaches the theoretical prediction Eq. (30) only for large fracture densities $\rho' = \rho_3' \gtrsim 20$. Close to the percolation threshold, K_2' strongly decreases, although it does not vanish because of the finite sample size. As discussed in Sec. III, the probability of percolation is about $1/2$ for $\rho_3' \approx 3$ and $L'=4$. However, Koudina *et al.* [5] showed that the dependence of K_2' on ρ_3' approaches a critical transition as the system size L' increases.

The permeability of polydisperse networks with $a=1.5$ is also presented in Fig. 3(a), for various R_m', δ_M, and L', as a function of the fracture density ρ_3'. The difference with respect to the monodisperse case is significantly reduced, compared to Fig. 2, thanks to the definition of K_2'; it is of the order of 20% for $\rho_3'=6$ and keeps decreasing for larger densities.

The difference between monodisperse and polydisperse systems increases near the percolation threshold where the statistical fluctuations and the finite size effects are important. Comparison of numerical results obtained for $R_m'=0.1$ and 0.01 shows that the influence of R_m' is not significant, and that the macroscopic permeability of fracture networks with the same value of ρ_3' remains proportional to $\rho\langle\sigma A_p\rangle$. The variations of K_2' with R_m' for fixed values of $\rho_3'=8$ and 12 are illustrated further in Fig. 4. One can see that it does not exceed the interval of statistical fluctuations.

In order to analyze the influence of the small fractures on flow, all fractures with R' smaller than some $R_{lim}' \geq R_m'$ have
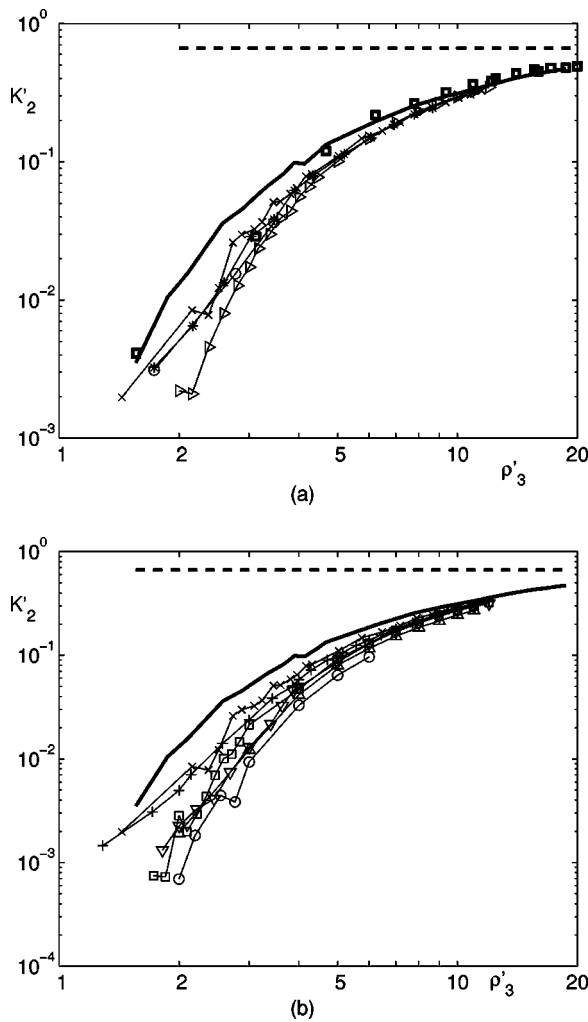
(a)

(b)

FIG. 3. Normalized effective permeability K_2' for nonperiodic networks of regular hexagons versus ρ_3'. Data in (a) are for $a=1.5$ and $R_m'=0.1$, $\delta_M=0.25$, $L'=4$ ($\times$), $R_m'=0.01$, $\delta_M=0.25$, $L'=4$ ($*$), $R_m'=0.01$, $\delta_M=0.167$, $L'=4$ ($\bigcirc$), and $R_m'=0.1$, $\delta_M=0.25$, $L'=6$ ($\triangleright$). Data in (b) are for $L'=4$ and $\delta_M=0.25$ with $a=1.5$, $R_m'=0.1$ ($\times$), $a=2$, $R_m'=0.1$ ($+$), $a=2.5$, $R_m'=0.1$ ($\square$), $a=2.5$, $R_m'=0.05$ ($\triangle$), $a=2.9$, $R_m'=0.1$ ($\triangledown$), $a=2.9$, $R_m'=0.05$ ($\bigcirc$). Data for monodisperse fracture networks with $\delta_M=0.25$ and $L'=4$ are given by the thick solid line for for nonperiodic systems and by ($\square$) for periodic networks. The thick broken line is the Snow equation Eq. (30).

been neutralized for flow in some networks initially generated with $R_m'=0.1$, and the macroscopic permeability of the resulting networks has been calculated. Figure 5 shows the results of numerical simulations performed for $N_r=25$ realizations. The permeability K is normalized by the permeability K_0 of the full network. For R_{lim}' up to 0.4, the decrements of the permeability and of the total fracture surface area (and therefore of the effective $\rho\langle\sigma A_p\rangle$) are roughly equal, whereas the number of fractures drops by about 75%. The effective density ρ_3' decreases even less than the surface area, since it is dominated by the large fractures. In this situation, 25% of the fractures account for 75% of the volumetric area and of the permeability.
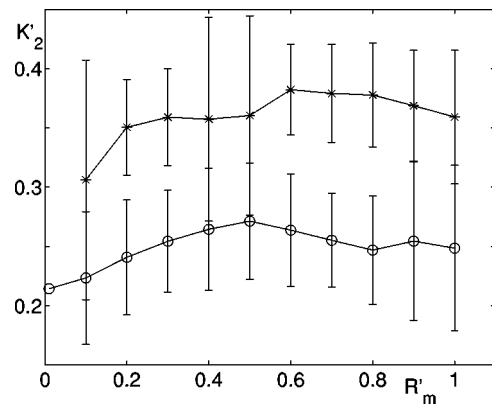

FIG. 4. Normalized permeability K_2' for nonperiodic networks of regular hexagons versus R_m' for $\rho_3'=8$ ($\bigcirc$), and 12 ($*$). Data are for $L'=4$ and $a=1.5$. Error bars represent the standard deviations corresponding to statistical fluctuations.

The stability of the numerical results relative to the grid discretization has been tested for $R_m'=0.01$. The macroscopic permeability calculated by using $\delta_M=1/4$ and $1/6$ is presented in Fig. 3(a). One can see that K is not affected by δ_M.

The variations of the numerical results due to the boundary conditions applied to the system are also illustrated in Fig. 5. The permeabilities of monodisperse fracture networks have been calculated when a macroscopic pressure gradient Eq. (10) was applied upon the periodic systems of fractures and have been compared to the data for the nonperiodic systems obtained with the boundary conditions Eq. (14). One can see that the difference between the two models is small for all the values of ρ_3' explored in the simulations.

The finite size effects have been discussed by Koudina *et al.* [5] for monodisperse networks. In this study, no systematic work has been done to explore the influence of L' on K. However, the curve for $L'=6$ in Fig. 3(a) is notably lower than the curves for $L'=4$, since the transition to percolation becomes sharper as the system size increases.

Let us now consider the influence of the power-law exponent a. The dimensionless permeability K_2' calculated for the
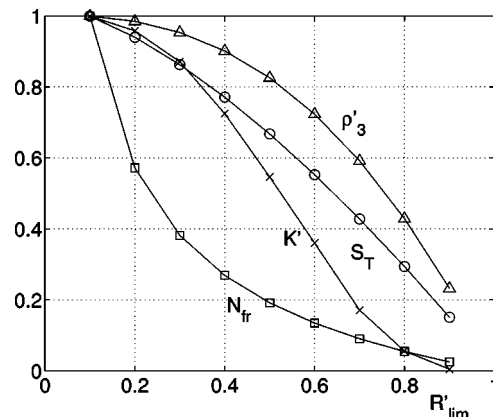

FIG. 5. Relative variations of the permeability K' ($\times$), total fracture surface S_T ($\bigcirc$), number of fractures N_{fr} ($\square$), and effective density ρ_3' ($\triangle$) for nonperiodic networks of regular hexagons with $\rho_3'=5.75$, $R_m'=0.1$, $a=1.5$ where all fractures with $R'<R_{lim}'$ are neutralized for flow.
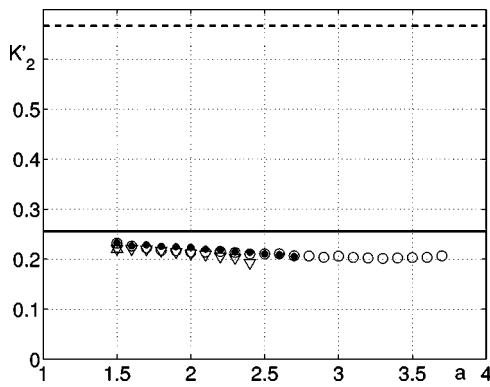
FIG. 6. Permeability K_2' for nonperiodic networks of regular hexagons versus a for $\rho_3'=8$. Data are for $L'=4$ with $R_m'=0.1$ ($\bigcirc$), 0.05 ($\triangledown$), or 0.01 ($\triangle$), and $L'=6$ with $R_m'=0.1$ ($\bullet$). The thick solid line corresponds to the monodisperse fracture networks, and the thick broken line is the Snow Eq. (30).

networks with $a=1.5$, 2, 2.5, and 2.9 is displayed in Fig. 3(b). For large fracture network densities $\rho_3'>4$ and a constant cutoff $R_m'=0.1$, K_2' is nearly insensitive to a, with variations within about 10%. For lower densities, the transition to zero permeability is sharper for the larger exponents $a=2.5$ and 2.9 than for the smaller ones $a=1.5$ and 2. This is because the larger a, the more small fractures contribute to the network connectivity and permeability; thereby, the effective size of the system increases and the finite size effects are reduced. Accordingly, the smoothest decay of K_2' is observed for the monodisperse networks. For large a, a residual influence of R_m' on K_2' is observed in Fig. 3(b). The network permeability is slightly smaller for $R_m'=0.05$ than in the case $R_m'=0.1$.

The efficiency of the combination Eq. (29) for the gathering of the results for different polydisperse fracture networks is summarized in Fig. 6. The normalized permeability K_2' is presented as a function of a for the same value $\rho_3'=8$; it slightly decreases from 0.2324 to 0.2025 with increasing a, but remains within 20% of the value $K_2'=0.2556$ derived for the monodisperse networks with the same ρ_3'. For such dense networks, the variations of R_m' and L' have little influence on K_2' in the range of a used in the simulations.

Finally, numerical data obtained for networks of polygons of various shapes, namely, squares, hexagons, and 20-gons, are shown in Fig. 7. The macroscopic permeability K of these systems for the same fracture number density ρ strongly depends on the fracture shape. However, the combined use of the normalized permeability K_2' and of the dimensionless density ρ_3' allows again to gather all the data obtained for the various shapes.

In summary, the macroscopic permeability of polydisperse fracture networks with intermediate and large densities can be written as

$$K = \rho \langle \sigma A_p \rangle K_2'(\rho_3'). \tag{31}$$

The term $\rho \langle \sigma A_p \rangle$ represents the volumetric area of fractures, weighted by the individual fracture conductivities, and the dimensionless function $K_2'(\rho_3')$ accounts for the network con-
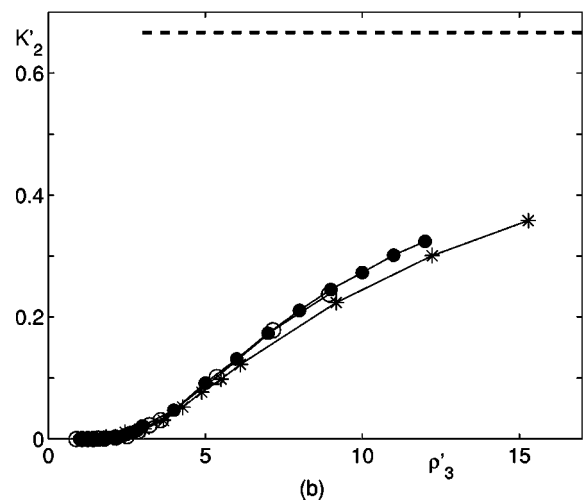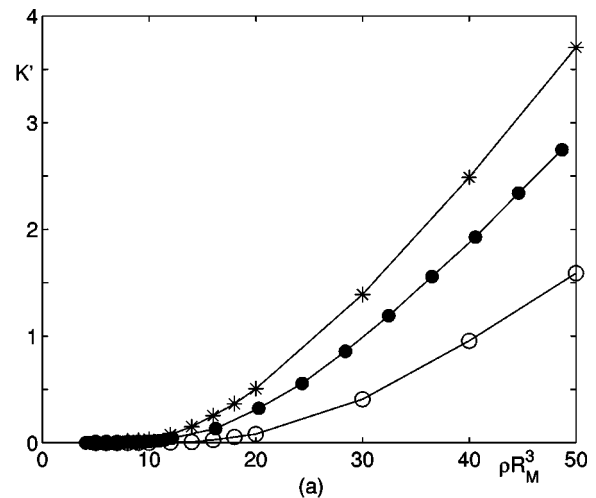

FIG. 7. Permeability K' versus ρ (a) and normalized effective permeability K_2' versus ρ_3' (b) for nonperiodic networks of regular polygons of various shapes for $L'=4$, $a=2.5$, and $R_m'=0.1$. Data are for squares ($\bigcirc$), hexagons ($\bullet$), and 20-gons ($*$). The thick broken line is the Snow Eq. (30).

nectivity and incorporates the influences of the fracture shape and of the fracture size distribution. Unsurprisingly, it is a function of the same quantity ρ_3' that controls the network percolation. This model is a direct extension of the corresponding result of Koudina *et al.* [5] about monodisperse fracture networks.

It should be noted that, given the fracture shape and R_M, $\rho \langle A_p \rangle$ is unequivocally related to ρ_3' when the exponent a is in the range $1<a<3$ and $R_m' \ll 1$, since both moments $\langle R^2 \rangle$ and $\langle R^3 \rangle$ are then insensitive to R_m, and the model Eq. (31) actually depends on a single parameter. However, this is not true when R_m' is not vanishingly small or when $a>3$. The two terms in Eq. (31) are then a natural and convenient way to account for the independent effects of the exponent and of the lower cutoff of the fracture size distribution.

Most calculations in this work have been conducted for $a<3$, and the model proves successful in this range even for nonvanishing R_m. As illustrated in Figs. 3, 4, 6, and 7, all the data for $0.01 \leq R_m' \leq 1$, $1.5 \leq a \leq 2.9$, and various fracture

shapes are represented by Eq. (31) within at most 20%, as soon as $L/R_M \geqslant 4$ and $\rho_3' \geqslant 4$. Exponents larger than 3 have not been systematically investigated but one case with $R_m' = 0.1$ and $\rho_3' = 8$ is considered in Fig. 6; K_2' does not vary when a is increased up to 3.7, which means that these data are indeed accurately represented by Eq. (31). It may seem disturbing that in the range $3 < a < 4$ the permeability results from the product of a term controlled by the smallest fractures, through $\langle R^2 \rangle$, and a term controlled by the largest ones, through $\langle R^3 \rangle$, but it should be remembered that Eq. (31) is proposed for moderate or large densities, i.e., for well connected networks.

For smaller densities, significant size effects are observed for the sample sizes that have been used in this study, which have not been systematically investigated. Still, we can formulate the general statement that these size effects decrease when the exponent a increases, because the role played by small fractures becomes more important.

Finally, when $a > 4$, both moments $\langle R^2 \rangle$ and $\langle R^3 \rangle$, i.e., the volumetric surface area and the network connectivity, are controlled by R_m, and large fractures are uncommon. Hence, although such networks have not been considered at all in this work and we do not have numerical data to support it, we can conjecture that they behave essentially like monodisperse networks of fractures with size R_m, and therefore that the model Eq. (31) is still applicable. A similar statement is possible for $a < 1$, since small fractures are then not numerous enough to play a significant role. Therefore, if this was verified, Eq. (31) would be a quite general and useful result which would provide a reasonable estimate of the network permeability for any range and exponent of the fracture size distribution.

V. VARIABLE FRACTURE CONDUCTIVITIES

It has been shown in the previous section that the macroscopic permeability of the polydisperse fracture networks with constant conductivity is proportional to the fracture surface density. An extension of this result to the case of variable fracture conductivity is discussed in this section.

A. Polydisperse networks

In natural fracture systems, geometrical apertures may vary over a wide range. These variations influence the fracture conductivity distribution as can be seen in the classical cubic law Eq. (15).

Fracture lateral sizes and apertures are in many cases positively correlated. When both characteristics follow power-law distributions, a scaling relationship can be tentatively written as

$$b = FR^\kappa. \tag{32}$$

From the existing data in the literature, one can find that the scaling exponent κ varies between 0.5 and 2 [28–32].

In order to obtain the distribution of fracture conductivities, it is assumed in this study that the fracture hydraulic conductivity σ is related to its mean geometrical aperture b via Eq. (15). In many cases, this relation is not exactly sat-

isfied for rough walled fractures, but it can be used for a first estimate of a fracture hydraulic aperture.

The scaling relationship Eq. (32) and the cubic law Eq. (15) imply

$$\sigma' = R'^\beta, \tag{33}$$

where $\beta = 3\kappa$, with a possible range of variation $1.5 < \beta < 6$. The value of the exponent β (or κ) may depend on the physical origin of the fracture system as well as on its history [33–36]. However, any detailed discussion of this question is beyond the scope of this study, and the model Eq. (33) is used here in a straightforward manner with $\beta = 1.5$, 3, and 6.

Note that the case of a variable conductivity along the fracture surface has not been addressed in the present study.

Figure 8(a) shows the numerical results obtained for fracture networks with $a = 1.5$ and various exponents β. The macroscopic permeability K' of polydisperse networks is substantially influenced by the value of the exponent β. However, the results are nicely gathered when the ratio Eq. (29) is used with the weighted fracture surface density $\rho \langle \sigma A_p \rangle$. When β varies from 0 to 3, K_2' remains very close to the data obtained for identical fracture conductivities. A substantial departure from this case is observed for $\beta = 6$. Note that K_2' starts increasing with β, and then decreases. These results can be explained by the fact that for $a = 1.5$ the network percolation is mainly due to large fractures. If the fracture conductivities are correlated with their sizes, a gradual increase of β from 0 to moderate values "switches off" small fractures which do not contribute significantly to the overall flow. When β is increased further, larger and larger fractures are progressively neutralized, and the macroscopic permeability decreases. Note that this tendency is partly hidden by the fact that the macroscopic permeability is normalized by the factor of $\rho \langle \sigma A_p \rangle$ which decreases with increasing β.

The numerical data for the networks with the exponent $a = 2.9$ are presented in Fig. 8(b). The influence of β is much more pronounced when compared to Fig. 8(a) with $a = 1.5$; this influence cannot be reduced by the use of K_2'. It is interesting to note that for small fracture densities the numerical data for various β are close to one another. In this range of densities, the large fractures are rare events and the network is composed mostly by small fractures which have similar sizes, and a variation of fracture conductivities results in a uniform global increase or reduction of fluid velocities, without flow redistribution. For large densities, some large fractures provide connections between various parts of the system and ensure the total flow rate even when small fractures are "switched off."

However, both K and $\rho \langle \sigma A_p \rangle$ are affected by the variations of fracture conductivities, and their dependence on β is not the same, so the combination K_2' slightly increases at first with β and then decreases gradually. Figure 9 shows the normalized permeability K_2' as a function of β for $a = 1.5$ and 2.9 when ρ_3' is kept constant. A nonmonotonic behavior of K_2' with β is well observed; it is more pronounced for $a = 2.9$.

We may conclude from these results that Eq. (31) is also successful in representing the permeability of polydisperse fracture networks with correlated individual fracture size and
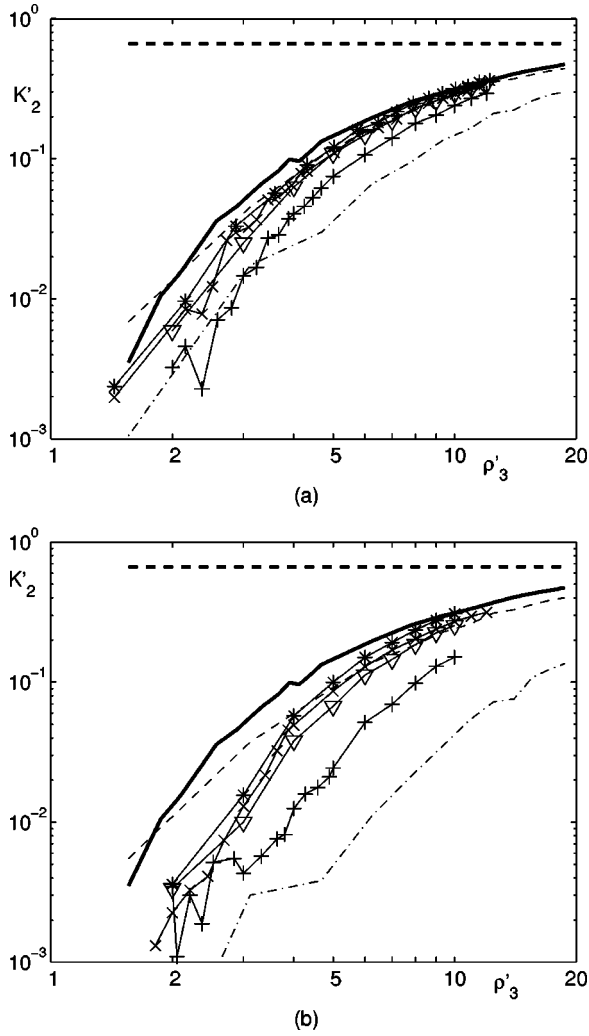
(a)

(b)

FIG. 8. Normalized effective permeability K_2' for nonperiodic networks of regular hexagons versus local conductivity versus ρ_3' for $L'=4$, $R_m'=0.1$, $a=1.5$ (a) or $a=2.9$ (b). Data are for $\beta=0$ ($\times$), 1.5 ($*$), 3 (∇), and 6 ($+$). Broken and dashed-dotted lines are for monodisperse systems with verying local conductivity, model Eqs. (34) and (35), for $\sigma_{min}'=0.032$, $\zeta=0$, (a) or $\zeta=0.9333$ (b) and $\sigma_{min}'=10^{-6}$, $\zeta=0.75$ (a) or $\zeta=0.9833$ (b), respectively. Data for monodisperse fracture networks are given by the thick solid line. The thick broken line is the Snow Eq. (30).

conductivity, when $\beta \lesssim 3$, and at least in the investigated range of the exponent a, thanks to the use of the statistical moment $\langle \sigma A_p \rangle$. Note that $\beta=3$ already corresponds to a fairly wide range of σ', from 10^{-3} to 1 if $R_m'=0.1$. However, the very steep dependence of σ on R with $\beta=6$ does not fit in this model. Finally, the case of size-dependent fracture conductivities with scaling exponents a larger than 3 has not been investigated.

B. Comparison with monodisperse networks

In this section we compare the macroscopic permeabilities of polydisperse networks with fracture conductivities distributed according to Eq. (33) to those of monodisperse
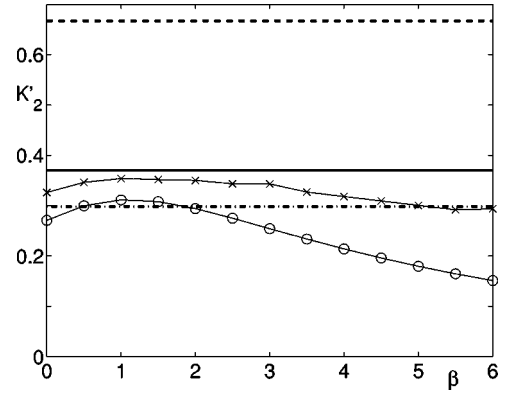

FIG. 9. Normalized permeability K_2' for nonperiodic networks of regular hexagons versus β. Data are for $\times$ ($a=1.5$, $L'=4$, $R_m'=0.1$, $\rho_3'=16$); $\bigcirc$ ($a=2.9$, $L'=4$, $R_m'=0.1$, $\rho_3'=10$). The thick solid and dotted-dashed lines correspond to monodisperse fracture networks for $\rho_3'=16$ and $\rho_3'=10$, respectively. The thick broken line is the Snow Eq. (30).

fracture systems with fracture conductivities following the power-law distribution

$$n(\sigma') = \frac{\zeta-1}{\sigma_{min}'^{1-\zeta}-1} \sigma'^{-\zeta}, \tag{34}$$

where the normalization constant is chosen so that $\sigma_{max}'=1$. This might be of practical interest, first because the treatment of the latter situation is numerically much less demanding and also because some field acquisition techniques such as line surveys can provide area-weighted fracture aperture distributions, but no information regarding the fracture size distribution [37].

In order to set a common basis for the comparison, the value of σ_{min}' in this simulation is set to the value $R_m'^{\beta}$ used in the previous one. The area-weighted fracture conductivity distributions should also be the same in both systems. This is true when

$$\zeta = \frac{a-3}{\beta} + 1 \tag{35}$$

Then the surface-weighted mean fracture conductivity is equal in both models:

$$\langle \sigma' \rangle * = \frac{\langle \sigma' A_p' \rangle}{\langle A_p' \rangle} = \frac{(a-3)(R_m'^{\beta+3-a}-1)}{(a-3-\beta)(R_m'^{3-a}-1)}. \tag{36}$$

The macroscopic permeability K_2' is compared for both systems for the same value of the fracture density ρ_3'; this means that the total fracture surface is not the same in the monodisperse and polydisperse networks.

Figure 8(a) presents the results for polydisperse networks with $a=1.5$ and for monodisperse networks with varying fracture conductivity. For $\beta=1.5$ which corresponds to $\sigma_{min}'=0.032$, the predictions of the macroscopic permeability by both models are close enough, while for $\beta=6$, $\sigma_{min}'=10^{-6}$ they differ significantly.

The simulation data for $a=2.9$ are shown in Fig. 8(b). It can be seen that for $\beta=1.5$, $\sigma_{min}'=0.032$, the prediction is

fairly good, while for $\beta=6$, $\sigma'_{\min}=10^{-6}$, the monodisperse networks significantly underestimate the permeability.

Hence, the monodisperse fracture network model with variable conductivity is shown to mimic the behavior of polydisperse systems if they have the same fracture conductivity distributions in surface and for small values of β only. It should be noted that for small fracture densities, the model Eqs. (34) and (35) gives reasonable predictions, even when $\beta=6$, but the difference increases with increasing ρ'_3.

VI. DISCUSSION AND CONCLUSIONS

Numerical simulations of steady flow in fracture networks with a power-law distribution of fracture sizes show that the hydraulic behavior of such networks varies substantially with the contrast between minimal and maximal fractures radii as well as with the exponent a. However, a unified description of the macroscopic permeability K of polydisperse networks can be proposed as

$$K = \rho \langle \sigma A_p \rangle K'_2(\rho'_3). \tag{37}$$

This model involves two factors. The extensive term $\rho \langle \sigma A_p \rangle$ is a measure of the network density, weighted by the individual fracture conductivities. The dimensionless function K'_2 is fairly universal, and the influence of the fracture shape and of the parameters (a, R'_m) of their size distribution are incorporated in the dimensionless density ρ'_3. It was shown in Sec. IV B that this relation is valid for all a in the range $1.5 < a < 3$ and does not vary with R'_m and the fracture shape. It was also conjectured that it is applicable for any value of the exponent a.

In the case of varying fracture conductivity σ, Eq. (37) holds for $a \lesssim 3$ and for moderate contrasts between $\sigma_{\min}$ and $\sigma_{\max}$, which corresponds to small or moderate values of the exponent β in the scaling relation Eq. (33). It breaks down, however, when β increases up to 6, and exponents a larger than 3 have not been investigated with varying fracture conductivities.

Near the percolation threshold, K'_2 approaches zero with fluctuations due to finite size effects, whose amplitude depends on a and on the contrast of fracture sizes in the network. For large densities, K'_2 slowly tends to the value $2/3$ predicted by Snow's model Eq. (30), although it is always smaller than this prediction for finite densities; the same phenomenon was observed for monodispersed networks [5]. This is partly due to the fact that not all the fractures contribute to the flow, especially for low fracture density, but also to nonuniformity of the flux distribution among the fractures as well as to the flow interactions between them, since both factors violate the assumptions leading to Eq. (28).

In view of the universality of Eq. (31), and of its high practical interest, it may be desirable to model it by an analytical formula, which could be easier to use than the tabulated data in Fig. 3(b) or Fig. 8(a). Two such models are proposed here.

An approximate expression for the permeability K'_2 can be proposed for large fracture densities by using a numerical fit. The effective medium model developed by Hestir and Long [27] for two-dimensional networks shows that the ratio
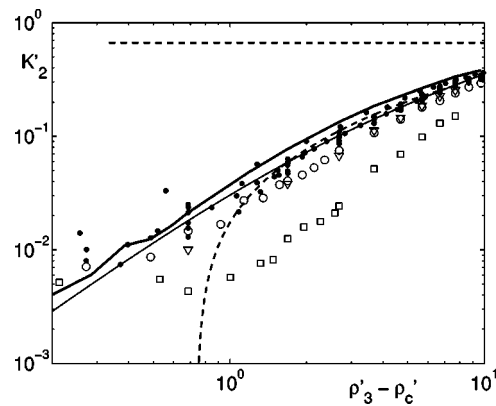

FIG. 10. Normalized effective permeability K'_2 for nonperiodic networks of regular hexagons versus $\rho'_3 - \rho'_c$ for $\rho'_c = 2.31$. Black dots ($\bullet$) correspond to the numerical data for $\beta=0$ with $a=1.5$, 2.0, 2.5, or 2.9, $\beta=1.5$ with $a=1.5$ or 2.9, and $\beta=3$ with $a=1.5$. Other symbols are for $\beta=3$ and $a=2.9$ ($\triangledown$), $\beta=6$ and $a=1.5$ ($\circ$) or $a=2.9$ ($\square$). In all cases, $R'_m=0.1$ and $L'=4$, except for $a=1.5$, $\beta=0$ with $L'=6$. Data for periodic monodisperse fracture networks are given by the thick solid line. The thick broken line is the Snow Eq. (30). The thin solid line is Eq. (42). The thin broken line is the prediction of Eq. (38).

$1/(1-K/K_{Sn})$ increases linearly with increasing ρ'_3 when ρ'_3 tends to infinity. A least squares fit of all the numerical data for three-dimensional polydisperse networks with $R'_m=0.1$, $\beta=0$, $a=1.5$ to 2.9, the largest sample size available ($L'=4$, except for $a=1.5$, with $L'=6$), and $\rho'_3 \geq 2.5$ yields

$$K'_2 \approx \frac{2}{3}\left[1 - \frac{1}{C_1(\rho'_3 + C_2)}\right], \quad C_1 = 0.10, \quad C_2 = 6.6. \tag{38}$$

This two-parameter fit is shown in Fig. 10 in comparison with the numerical results. A good agreement is observed with the data for $\beta=0$, for densities $\rho'_3 \geq 3.5$. Concordance is also good with the data for $\beta=1.5$ ($a=1.5$ and 2.9) and for $\beta=3$ ($a=1.5$), which were not used in the determination of the coefficients of the least squares fit. Only the most extreme cases with $a=2.9$ and $\beta=3$ or with $\beta=6$ deviate significantly from Eq. (38).

The second model is a generalization of a result of Koudina *et al.* [5] Close to the percolation threshold, the conductivity of a site or bond lattice is known to vanish according to a power law [24]. In continuum percolation, a similar scaling law is expected,

$$K \propto (\rho'_3 - \rho'_c)^t. \tag{39}$$

The exponent $t=2.0$ is generally accepted for lattice percolation in three dimensions. However, in continuum percolation this exponent may depend upon the geometrical model. Koudina *et al.* [5] analyzed monodisperse fracture networks and showed by considering large samples very close to the critical density that the power law Eq. (39) is well satisfied with an exponent close to the usual lattice value.

Furthermore, Koudina *et al.* [5] showed that a similar power law with an exponent 1.57 describes fairly accurately the network permeability in a wide range $3.5 \leq \rho'_3 \leq 16$. They

conjectured that this dependence is merely a transition between the critical power law near the percolation threshold and the linear growth Eq. (28).

Since such a relation is of interest for practical purposes, the same kind of fit was attempted for polydisperse networks. We used as the critical density for finite polydisperse networks the value $\rho'_{3c} = \rho'_c = 2.31$, which is a slight improvement on the estimate of the percolation threshold for monodisperse systems of hexagons derived by [4]; it is extrapolated for $L' = \infty$ via the finite size scaling method Eq. (17), based on data for L' up to 20 instead of 8 in [4]. The notation t in Eq. (39), which is reserved traditionally for the critical exponent near the percolation threshold, is kept regardless of the fact that it will be derived from the data obtained with larger network densities.

Substituting Eq. (6c) in Eq. (37), the permeability K can be written in the form

$$K = \frac{\langle \sigma A_p \rangle}{v_{ex} \langle R^3 \rangle} \Phi(\rho'_3), \quad \Phi = \rho'_3 K'_2. \tag{40}$$

Writing the scaling law Eq. (39) as

$$\Phi = C_3 (\rho'_3 - \rho'_c)^t \tag{41}$$

and fitting the same permeability data set as for Eq. (38) in the range $\rho'_3 - \rho'_c > 1.5$, yields $C_3 = 0.101$ and $t = 1.63$. Hence, the resulting model reads

$$K'_2 = \frac{C_3}{\rho'_3} (\rho'_3 - \rho'_c)^t, \quad C_3 = 0.10, \quad t = 1.6. \tag{42}$$

It is shown in Fig. 10, and the agreement between the predictions and the numerical data is good in the range $0.4 < \rho'_3 - \rho'_c < 10$. There is a wide interval of ρ'_3 where the predictions of both models Eqs. (38) and (42) are very close to one another. However, for large fracture densities, where a constant K'_2 is expected , the latter model predicts $K'_2 \propto (\rho'_3)^{t-1}$, which imposes a limit for the applicability of Eq. (42).

Just like the first model Eq. (38), Eq. (42) is also successful in representing the numerical data for networks with variable individual fracture conductivities, except for the most extreme cases with $(a=2.9, \beta=3)$ or with $\beta=6$.

Figure 11 shows in more detail the macroscopic permeability in a few cases. K', instead of K'_2, is plotted versus $\rho'_3 - \rho'_c$ in order to make the power law apparent. Thus, the data do not all fall on a single curve since they are not normalized by the volumetric surface area, but they are arranged along straight lines over nearly a decade in this log-log plot.

The exponents t estimated from these data by least squares fits in some of these cases are given in Table I. Since the power laws are fitted over slightly less than a decade, and because of the statistical noise, the estimations of t are sometimes imprecise. Nevertheless, the correlation coefficient r, which quantifies the quality of the fit, is always close to 1.
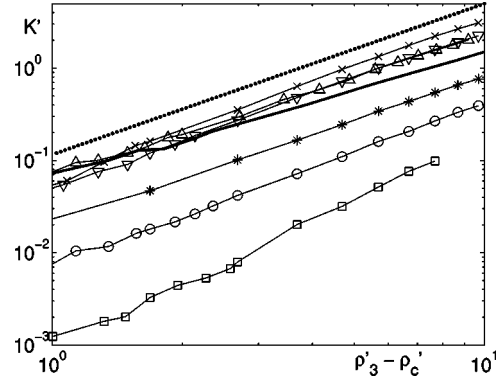

FIG. 11. Permeability K' for nonperiodic networks of regular hexagons versus $\rho'_3 - \rho'_c$ for $\rho'_c = 2.31$. The symbols correspond to $a=1.5$, $\beta=0$ ($\triangle$); $a=1.5$, $\beta=0$, $L'=6$ ($\triangledown$); $a=2.9$, $\beta=0$ ($\times$); $a=1.5$, $\beta=3$ ($\star$); $a=1.5$, $\beta=6$ ($\bigcirc$); $a=2.9$, $\beta=0$ ($\square$); the thick solid line corresponds to monodisperse fracture networks; $R'_m=0.1$ and $L'=4$ in all cases unless otherwise stated. The dotted line shows the slope $t=1.63$ corresponding to Eq. (42).

The error bars for t are 95% confidence intervals for the values of the exponent, resulting from the statistical fluctuations of the individual data.

The first three lines of Table I, for polydisperse networks with $\beta=0$ or 3, give very similar results, and exponents consistent with the global fit Eq. (42), as well as with the value of t obtained by Koudina *et al.* (5) in monodisperse samples with L' up to 10. In contrast, the exponent obtained here for monodisperse networks is abnormally low, because of the small sample size $L'=4$. The polydisperse networks, which contain only a few large fractures, are less sensitive to this finite size effect. Finally, and as already noted in Fig. 10, the results for polydisperse networks with varying fracture conductivities with $\beta=6$, especially when a is also large, do not fit in the same pattern as the others. However, the simulation results are too influenced by finite size effects to conclude whether or not this is due to a transition to another universality class.

TABLE I. Exponent t of the power law Eq. (42), with its 95% confidence interval, and associated correlation coefficient r, obtained by least squares fits of the data in Fig. 11 for $\rho'_3 - \rho'_c \geqslant 1.5$.

a	β	L'	t	r
1.5	0	6	1.62 ± 0.06	0.9990
2.9	0	4	1.66 ± 0.08	0.9993
1.5	3	4	1.58 ± 0.16	0.997
1.5	6	4	1.77 ± 0.16	0.9998
2.9	6	4	2.4 ± 0.4	0.998
Monodisperse		4	1.38 ± 0.07	0.9999
Monodisperse [5]		$4 \sim 10$	1.57	0.9994
Global, Eqs. (40)–(42)		$4 \sim 6$	1.63 ± 0.03	0.997

In summary, the two analytical formulas Eqs. (38) and (42) are equally successful in representing all the numerical data for intermediate and large network densities, except for very large conductivity exponents β, and together with the expression Eq. (37) they provide a general, simple, and fairly accurate estimate of the permeability of polydisperse fracture networks.

[1] M. Sahimi, *Flow and Transport in Porous Media and Fractured Rock* (VCH, New York, 1995).

[2] P.M. Adler and J.-F. Thovert, *Fractures and Fracture Networks* (Kluwer Academic Publishers, Dordrecht, Netherlands, 1999).

[3] National Research Council, *Conceptual Models of Flow and Transport in the Fractured Vadose Zone* (National Academy Press, Washington, DC 2001).

[4] O. Huseby, J.-F. Thovert, and P.M. Adler, J. Phys. A **30**, 1415 (1997).

[5] N. Koudina, R. Gonzalez Garcia, J.-F. Thovert, and P.M. Adler, Phys. Rev. E **57**, 4466 (1998).

[6] I.I. Bogdanov, V.V. Mourzenko, J.-F. Thovert, and P.M. Adler, Water Resour. Res. **39**, 1023 (2003).

[7] I.I. Bogdanov, V.V. Mourzenko, J.-F. Thovert, and P.M. Adler, Phys. Rev. E **68**, 026703 (2003).

[8] I. Balberg, C.H. Anderson, S. Alexander, and N. Wagner, Phys. Rev. B **30**, 3933 (1984).

[9] G. Yielding, J. Walsh, and J. Watterson, First Break **10**, 449 (1992).

[10] C.H. Scholz, N.H. Dawers, J.-Z. Yu, M.H. Anders, and P.A. Cowie, J. Geophys. Res., [Solid Earth] **98**, 21,951 (1993).

[11] C. Castaing, M.A. Halawani, F. Gervais, J.P. Chiles, A. Genter, B. Bourgine, G. Ouillon, J.M. Brosse, P. Martin, A. Genna, and D. Janjou, Tectonophysics **261**, 291 (1996).

[12] N.E. Odling, J. Struct. Geol. **19**, 1257 (1997).

[13] C.E.R. Line, D.B. Snyders, and R.W. Hobbs, J. Struct. Geol. **19**, 687 (1997).

[14] B. Berkowitz, Adv. Water Resour. **25**, 861 (2002).

[15] C.E. Renshaw, Water Resour. Res. **35**, 2661 (1999).

[16] N.E. Odling, in *Hydrogeology of Hard Rocks, Memories of the XXIVth Congress of IAH, Oslo 1993*, edited by Sheila and David Banks (Geological Survey of Norway, Trondheim, 1993), p. 290.

[17] J.-R. de Dreuzy, P. Davy, and O. Bour, Water Resour. Res. **38**, 1276 (2002).

[18] E. Bonnet, O. Bour, N.E. Odling, P. Davy, I. Main, P. Cowie, and B. Berkowitz, Rev. Geophys. **39**, 347 (2001).

[19] A.R. Piggott, J. Geophys. Res., [Solid Earth] **102**, 18121 (1997).

[20] B. Berkowitz and P.M. Adler, J. Geophys. Res., [Solid Earth] **103**, 15 339 (1998).

[21] E. Charlaix, E. Guyon, and N. Rivier, Solid State Commun. **50**, 999 (1984).

[22] O. Bour and P. Davy, Water Resour. Res. **34**, 2611 (1998).

[23] J.-R. de Dreuzy, P. Davy, and O. Bour, Phys. Rev. E **62**, 5948 (2000).

[24] D. Stauffer and A. Aharony, *Introduction to Percolation Theory* (Taylor and Francis, Bristol, PA, 1992).

[25] D.T. Snow, Water Resour. Res. **5**, 1273 (1969).

[26] M. Oda, Y. Hatsuyama, and Y. Ohnishi, J. Geophys. Res., [Solid Earth Planets] **92**, 8037 (1987).

[27] K. Hestir and J.C.S. Long, J. Geophys. Res., [Solid Earth Planets] **95**, 21 565 (1990).

[28] J.M. Vermilye and C.H. Scholz, J. Struct. Geol. **17**, 423 (1995).

[29] A. Gudmundsson, S.S. Berg, K.B. Lyslo, and E. Skurtveit, J. Struct. Geol. **23**, 343 (2001).

[30] C.M. Teixeira da Silva, M.A. Fonseca, and A.R. da Costa, Rev. Bras. Geosci. **31**, 247 (2001).

[31] J.D. Johnston and K.J. W. McCaffrey, J. Struct. Geol. **18**, 349 (1996).

[32] T. Walmann, A. Malthe-Sorenssen, J. Feder, T. Jossang, P. Meakin, and H.H. Hardy, Phys. Rev. Lett. **77**, 5393 (1996).

[33] M. Madadi and M. Sahimi, Phys. Rev. E **67**, 026309 (2003).

[34] Y. Meheust and J. Schmittbuhl, Geophys. Res. Lett. **27**, 2989 (2000).

[35] Y. Meheust and J. Schmittbuhl, J. Pure Appl. Geophys. **160**, 1023 (2003).

[36] V. Mourzenko, J.-F. Thovert, and P.M. Adler, Transp. Porous Media **45**, 89 (2001).

[37] S. Sisavath, V. Mourzenko, P. Genthon, J.-F. Thovert, and P.M. Adler, Geophys. J. Int. **157**, 917 (2004).